


Resonant excitation of very high gradient plasma wakefield accelerators by optical-period bunch trains

P. Manwani^{1,*}, N. Majernik¹, M. Yadav,^{1,2,3} C. Hansel,¹ and J. B. Rosenzweig¹

¹Department of Physics and Astronomy, UCLA, Los Angeles, California 90095, USA

²Department of Physics, University of Liverpool, Liverpool L69 7ZX, United Kingdom

³Cockcroft Institute, Warrington WA4 4AD, United Kingdom

 (Received 19 March 2020; revised 2 April 2021; accepted 28 April 2021; published 18 May 2021)

The use of a periodic electron beam bunch train to resonantly excite plasma wakefields in the quasilinear (QNL) regime has distinct advantages over employing a single, higher charge bunch. Resonant QNL excitation can produce plasma electron blowout using a small charge per pulse if the beam emittance beams are very low. The local density perturbation in such a case is extremely nonlinear, achieving total rarefaction, yet the resonant response of the plasma electrons at the plasma frequency is preserved. The needed electron beam pulse train with interbunch spacing equal to the plasma period can be produced via inverse free-electron laser bunching. As such, in achieving resonance with a laser wavelength of a few microns, a high plasma density is employed, with the attendant possibility of obtaining extremely large wakefield amplitudes, near 1 TV/m for FACET-II parameters. In this article, we use particle-in-cell (PIC) simulations to study the plasma response, the beam evolution including density modulation, and the instabilities encountered when using a bunched-beam scheme to resonantly excite waves in a dense plasma.

DOI: [10.1103/PhysRevAccelBeams.24.051302](https://doi.org/10.1103/PhysRevAccelBeams.24.051302)

I. INTRODUCTION

In a beam-driven plasma wakefield accelerator (PWFA), electromagnetic fields are excited by an intense, relativistic particle beam driver. An oscillating plasma wave trails behind the driver, and the associated wave fields can be utilized to accelerate charged particles, most commonly electrons. Indeed, the acceleration of electrons in a PWFA is a highly attractive scenario, due to high accelerating gradients, and the possibility of stable, linear transverse motion, particularly in the presence of a nonlinear plasma response [1], as discussed in detail below. A trailing, accelerating electron bunch is termed a witness beam in this scheme. While the plasma wakefield is most commonly excited by a single, short beam pulse, the use of a pulse train as the driver instead of a single pulse, to resonantly excite the wakefield, may permit new methods of efficiency enhancement and the excitation of large amplitude wakes. As an example of efficiency increases, in this scenario, the driving and accelerating beams may be interleaved, giving the opportunity to strongly augment the

beam loading and increase the energy extraction from the wave.

The pulse trains needed for this resonant drive scheme in the relevant range of periodicities can be produced through inverse free-electron laser (IFEL) bunching, as demonstrated recently in experiments performed at the Linac Coherent Light Source (LCLS) at the SLAC National Accelerator Laboratory [2]. Resonant excitation requires stable wakes of a known frequency which, given the presence of strong nonlinear plasma effects such as wave-breaking and amplitude-dependent wave frequency, is not straightforward in the most often-employed PWFA blowout regime [3,4].

To overcome these frequency-detuning issues while preserving the advantages of the blowout regime [1], we investigate here resonant excitation by trains with bunch-to-bunch spacing on the order of femtoseconds, in the particularly advantageous *quasilinear regime* (QNL). In the QNL regime, plasma electron blowout is achieved, but with very low emittance beam pulses possessing a small charge per pulse. In this case, the plasma electrons are rarefied from the beam path (an essential characteristic of the blowout regime), which is a nonlinear process arising from the strong local charge density perturbation employed for plasma wave excitations. Specifically, the plasma is very underdense—with the beam density much larger than that of the plasma, $n_b \gg n_0$. In QNL operation, the beam is confined to a radial region significantly smaller than the plasma wavelength, $\lambda_p = 2\pi/k_p$, where $k_p = \omega_p/c = \sqrt{4\pi r_e n_0}$. In this case,

*pkmanwani@gmail.com

Published by the American Physical Society under the terms of the *Creative Commons Attribution 4.0 International* license. Further distribution of this work must maintain attribution to the author(s) and the published article's title, journal citation, and DOI.

the global plasma wave disturbance, and thus the wake as a whole, is governed by an approximately *linear* frequency response, yielding the constant, nearly amplitude-independent frequency wave. The plasma waves may thus still be excited in a resonant fashion through bunch trains that have the same period as linear plasma waves, $\lambda_L = \lambda_p$.

Techniques for creating the electron bunch trains at optical to mm scale needed for this scheme are an active area of investigation. Phase space masking techniques exploiting the transverse dispersion of energy-chirped beams can produce trains with interbunch spacing on the order of hundreds of μm , as demonstrated by recent QNL regime experiments at the BNL ATF [4,5]. However, to produce bunch spacing of a few μm , and thus the possibility of very large electric fields in the plasma wave, an IFEL-based approach is much more feasible. To quantify the goal of obtaining large PWFA fields, a train with bunch-to-bunch spacing of $2 \mu\text{m}$ is resonant with a very high density plasma: $n_0 = k_p^2/4\pi r_e = 2.79 \times 10^{20} \text{ cm}^{-3}$. This density, in combination with assumptions of quasilinear waves approaching wave-breaking amplitude, $E_{\text{WB}} = m_e c^2 k_p$, implies extremely large-amplitude excited wakefields, up to TV/m, as discussed below.

Experimentally, a cryogenically cooled gas jet operated at many atmospheres of pressure may be used to produce the required density [6]. Matching the beam into such a dense plasma [7] requires an extremely short focusing beta function: $\beta_{\text{eq}} = \sqrt{2\gamma} k_p^{-1} < 100 \mu\text{m}$ for the 10 GeV beams foreseen at FACET-II [8]. This is a key challenge in the experimental realization of this scheme. A very high gradient (up to 700 T/m) permanent magnet quadrupole triplet [9] can begin to focus the beam into the plasma, with further focusing by an adiabatic ramping [7,10] of plasma density necessary to achieve the final, matched beta function. For example, a 3.2 pC microbunched ($2 \mu\text{m}$ period, 348 A peak current) beam with a normalized emittance of 50 nm rad [11] has a matched spot size, σ_x , of 13 nm comparable to a linear collider final focus [12]. At this size, the beam creates enormous radial electric fields, near 1 TV/m, which will ionize the gas atoms in a high field process termed the barrier suppression regime [13]. The beam parameters described are expected to be produced at SLAC's FACET-II facility [8] although modifications to the photoinjector (of the nature described in [11,14]) will be necessary, as well as an upgrade to the final focus system with high gradient quadrupole magnets [9], and the implementation of an IFEL buncher [15]. All of these upgraded capabilities have either been demonstrated or are currently under development. The experiments outlined in this paper have been formally approved for FACET-II with the SLAC experimental number E-317 assigned.

This article studies the physics issues attendant to this approach to resonant PWFA computationally, employing QUICKPIC [16], a three-dimensional quasistatic

particle-in-cell code, to explore both the general characteristics of this scheme as well as the specific case of E-317 experimental parameters. As such, we give a short description of the simulation approach to resolving the physical effects of interest. Due to the high plasma frequencies and short beam pulses involved in these simulations, the time step used in the numerical calculations is very small, as it is chosen as $5/\omega_p$. To reveal the relevant physical phenomena, the simulation's moving window is large, $(2.4 \mu\text{m})^2$ wide and $26 \mu\text{m}$ long, divided into $1024^2 \times 2048$ cells respectively; four simulation particles per cell of each species were used for the simulations running for short duration, i.e., $1000/\omega_p$, unless otherwise specified. The size of the simulation window and the particle per cell for the simulations running for a longer duration, i.e., $5000/\omega_p$ is specified below in the table containing the simulation parameters.

II. PERIODIC BUNCHING WITH IFEL

Introduced in 2004 [17], the inverse free electron laser (IFEL) technique for microbunching (periodic bunching at the optical scale), was proposed as a means of generating high peak current bunch trains. As the initial foreseen application was in SASE FELs, this process has also been termed "enhanced self-amplified spontaneous emission" bunching. Here, the same approach may be used to produce the optical-period bunch trains required for driving resonant beam-plasma interactions, while maintaining excellent control over the beam quality [18]. In this technique, the electron peak current is significantly increased by an interaction between the electron beam and a high peak power laser pulse in a magnetic wiggler. The wiggler period, λ_w , and wiggler parameter, $K_w = eB_w\lambda_w/(2\pi m_e c)$, where B_w is the peak magnetic field, are chosen such that $\lambda_L = (\lambda_w/2\gamma_b^2)(1 + K_w^2/2)$, where λ_L is the laser wavelength and γ_b is the relativistic factor for the average beam energy. An energy modulation at the laser wavelength λ_L is imparted on the electron beam, which is then converted into a density modulation in a magnetic chicane [15].

Using this method to produce the pulse train desired for a range of applications including resonantly excited PWFA has numerous advantages. Since the process can take place at relatively higher energy, space-charge induced emittance growth is suppressed. Further, since it takes place in a vacuum there is less degradation due to beam structure wakefield interactions; finally, due to the relatively modest bending needed, the effects of coherent synchrotron radiation are mitigated [19]. This has been demonstrated using a $2 \mu\text{m}$ laser with a $\lambda_w = 32 \text{ cm}$, variable strength ($K_w \leq 52$) wiggler in the x-ray laser enhanced attosecond pulse generation (XLEAP) project [2], illustrating the feasibility of microbunch creation in a case very close to that which is foreseen for FACET-II experiments.

III. RESONANT PLASMA WAKEFIELD EXCITATION

In a plasma wakefield accelerator, the plasma is initially set into motion by the forces associated with the electromagnetic fields of the driving particle bunch. In the linear regime, the resultant perturbation of the plasma density is small compared to n_0 . In contrast, if the beam is very dense, the plasma electrons are completely ejected from the beam channel, leaving a “bubble” in the density profile. In this case, one refers to the nonlinear (blowout) regime [1,20]. Unlike in the linear regime, with its nonideal, radially and temporally varying focusing fields, the blowout regime possesses a radial focusing field that is linear in r and constant along the length of the bubble [3]; the focusing is emittance preserving. Further, since the magnitude of its accelerating field is independent of radial position [1] in the blowout regime, there is no introduction of radially dependent energy spread, in contrast to the linear regime. These aspects of the transverse and longitudinal wakefields, respectively, facilitate the acceleration of high quality beams over long distances.

In general, however, the period of the excited plasma wave in the blowout regime is dependent on the charge density of the bunches [1], unlike the linear regime which depends only on the plasma density and beam axial velocity. Indeed, in the linear regime, the plasma response can be resonantly excited by a pulse train, with each bunch adding to the plasma wave via constructive superposition. Resonant PWFA excitation in the linear (overdense) regime has been experimentally demonstrated by modulating an electron beam into a train of microbunches spaced at a laser wavelength of $\lambda_L = 10.6 \mu\text{m}$ through an IFEL interaction at the BNL ATF facility [21]. This linear resonant excitation process may continue until the nonlinear regime is approached, and the resonance may break down due to the elongation of the plasma wave period [22]. The QNL regime, as noted above, exploits the advantages of both the linear and nonlinear regimes by employing low-emittance, tightly focused beams with relatively small charges. In this case, the local beam density can greatly exceed that of the surrounding plasma, while simultaneously having a smaller total charge than the relevant plasma electrons taking part in the interaction, thus allowing for blowout while still maintaining a quasilinear frequency response in the bulk plasma [23]. The blowout, or rarefaction, of the plasma electrons, leaves a nominally uniform ion column, giving linear focusing; it also gives acceleration independent of transverse offset inside of the rarefaction region. These properties represent significant advantages over the linear regime. We expand on the experimental phenomena encountered in an optically microbunched QNL PWFA in what follows.

The total plasma charge taking a direct part in the beam-plasma interaction is quantified by the number of electrons contained in a cubic plasma skin depth, $n_0 k_p^{-3}$. A useful

parameter for characterizing whether a resonant excitation is in the linear, QNL, or full blowout regime, respectively, is thus given by the normalized charge \tilde{Q} [24]:

$$\tilde{Q} = m \frac{N_b k_p^3}{n_0} = m 4\pi r_e k_p N_b, \quad (1)$$

where the factor m is the number of bunches in the train, N_b is the number of electrons in each bunch, and r_e is the classical electron radius. This parameter is the beam charge normalized to the relevant plasma electron charge. Indeed, in order to utilize this definition, each microbunch must be assumed to occupy a volume smaller than approximately k_p^{-3} , simultaneously obeying the conditions $k_p \sigma_x \ll 1$ and $k_p \sigma_z < 1$; this second criterion is already implied by the assumption of a resonant pulse train yielding efficient excitation.

The condition for the wakefield to be definitively in the blowout regime, in the case of a single bunch ($m = 1$), is met when $\tilde{Q} > 1$ which implies that $n_b > n_0$, independently of the values of $k_p \sigma_z$ and $k_p \sigma_x$, as long as they are less than unity. The parameter \tilde{Q} can, on the other hand, with knowledge of these beam parameters, be taken as a measure of the nonlinearities present in the beam-plasma interaction [24], such as period lengthening and wave steepening. With a resonant bunch train, the wake responses of the bunches should add linearly, so the total charge of the train is used to calculate \tilde{Q} , inspiring the introduction of the factor m above. This superposition is expected to hold true in the case of linear, resonant excitation, and also in the QNL regime. In the present study, the limits on resonance (the upper boundary associated with the QNL regime) for \tilde{Q} are explored. In particular, nonlinear detuning of the resonant frequency is expected as \tilde{Q} approaches or exceeds unity, moving past the QNL regime, and into the strong blowout regime.

The PIC simulations employed in this paper are carried out using a plasma density, $n_0 = 2.79 \times 10^{20} \text{ cm}^{-3}$, corresponding to a plasma wavelength, λ_p , of $2 \mu\text{m}$. Significantly, this density also implies a wave-breaking field (a guideline to the scale of the maximum wakefield amplitude obtainable), of $E_{\text{WB}} = 1.6 \text{ TV/m}$. The electron beams are assumed to have transversely symmetric Gaussian profiles with an energy of 10 GeV, consistent with FACET-II expectations. The charge and emittance for the microbunches are consistent with the results of Ref. [11], with each microbunch having a charge of 0.32 pC and 50 nm rad normalized emittance unless otherwise specified. This charge and periodicity imply that the beam before IFEL microbunching has an easily accessible peak current of 348 A [25]. The matched transverse spot size is calculated using $\sigma_x = \sqrt{\beta_{\text{eq}} \epsilon_{\perp}}$. The total beam charge differs for each case based on the number of microbunches employed, and is specified with the plots.

Typical distributions of the beam charge density, plasma electron density, and longitudinal electric fields found in

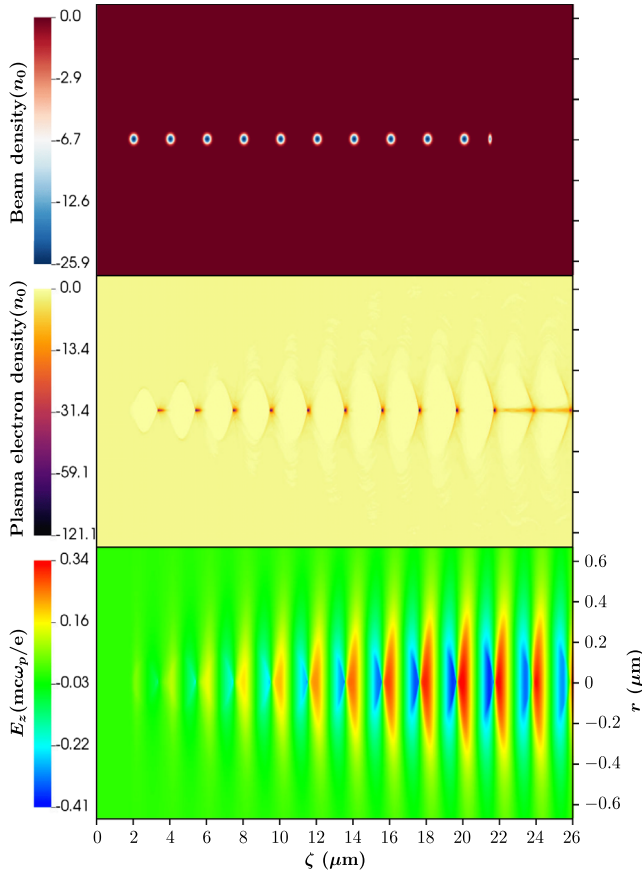


FIG. 1. PIC simulation snapshots of the beam charge density, plasma electron density, and longitudinal electric field for the ten bunches followed by a witness bunch (charge per driver bunch = 0.32 pC).

these studies are shown in Fig. 1. The simulations use a moving window approach and the parameter $\zeta = ct - z$ gives the Galilean transformation for describing the longitudinal dependence of particles and fields in the window. The longitudinal electric fields increase after each microbunch passage, as shown in Fig. 2(a). The regions of very high plasma electron density at the ends of each bubble region become increasingly narrow after every subsequent microbunch due to nonlinear wave breaking, as is shown in Fig. 2(b).

Due to the very large electric fields involved, the typical approximation of static plasma ions is no longer valid; their distribution evolves over the course of the periodic plasma excitation by the beam. The effects of ion motion on the plasma’s ion and electron densities distributions, as well as associated radial electric fields, are illustrated in Fig. 3. Given the presence of ion motion, each microbunch will experience notably different focusing fields, leading to the observed ramping effect on the beam density profile. The on-axis ion density increase further augments the focusing gradient near the axis. It also can lead to nonlinear transverse fields which may contribute to emittance growth for

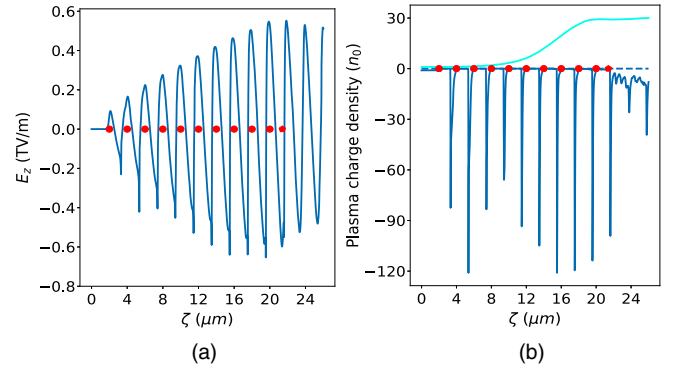


FIG. 2. The axial longitudinal electric field (a), plasma electron (dark blue) and ion (light blue) density (b) when using ten driver bunches (circle) (charge per driver bunch = 0.32 pC) and a witness bunch. Each bunch is separated by λ_p and has an initial transverse spot size of 13 nm.

beam distributions which extend beyond the radially localized ion density increase.

The system described above was simulated (see parameters of Table I) for a time equal to $\frac{5000}{\omega_p}$, i.e., a distance of about 1.59 mm. The resonant beam-plasma interaction remains stable for the entire duration of this simulation. The maximum energy change observed in the witness beam was 937 MeV, corresponding to an accelerating gradient of ~ 0.59 TeV/m; a reasonable fraction of wave breaking is achieved in the longitudinal field.

A. Variation with charge

The relationship between beam charge and the maximum field gradient for this scenario with a ten microbunch train is now considered. The beam’s transverse emittance in each of these cases was scaled linearly with the charge of the microbunch [26] while the longitudinal extent of each microbunch, σ_z , was kept constant. The simulations were

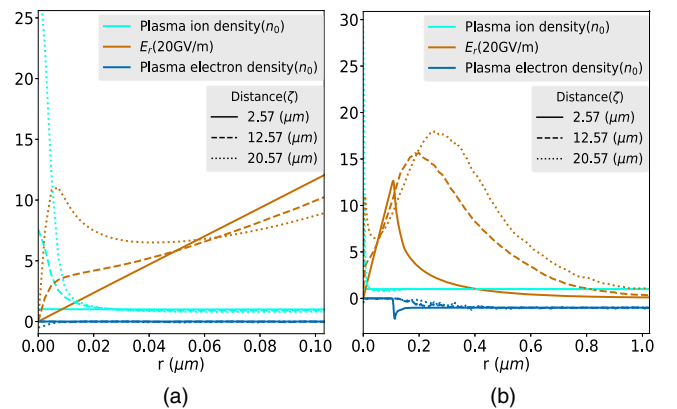


FIG. 3. The radial fields, plasma electron and ion densities inside the bubble cavity at three different ζ positions: (a) shows the region near axis in greater detail and (b) shows the longer range behavior.

TABLE I. Table of parameters for the simulation shown in Fig. 1.

Parameter	Value
Total beam charge, Q_b	3.2 pC
Beam energy, E_b	10 GeV
Number of bunches, m	10
Bunch length, σ_z	110 nm
Bunch spot size, σ_x	13 nm
Normalized transverse emittance, $\gamma\epsilon_\perp$	50 nm rad
Plasma ion species	H ⁺
Plasma density, n_0	$2.79 \times 10^{20} \text{ cm}^{-3}$
Plasma particles per cell	4
Simulation window	$(2.4 \mu\text{m})^2 \times 26 \mu\text{m}$
Resolution	$(2.34 \text{ nm})^2 \times 12.7 \mu\text{m}$

run for $t = \frac{1000}{\omega_p}$ i.e., a beam propagation distance of about 0.32 mm. The width of the simulation box was changed to 1.2, 4, 5, and 6 μm for beams with total charges of 0.8, 6.4, 12.8, and 25.6 pC, respectively. The axial longitudinal fields have notable spikes attributed to the presence of plasma density spikes near the tail of the bubble. To make sure that these field spikes are not considered in the estimation of the value and position of the maximum longitudinal fields, an equal weighted average of the longitudinal fields corresponding to 20 radial cells is used and the results are shown in Fig. 4. As the beam charge is increased, the maximum electric field increases, due to the plasma perturbation being commensurately larger. Another observed feature is that the plasma wake profile tends to be less sinusoidal and more sawtooth in form in the case of higher charges, a clear signature of the onset of wave nonlinearity. Due to such nonlinear effects, saturation of the

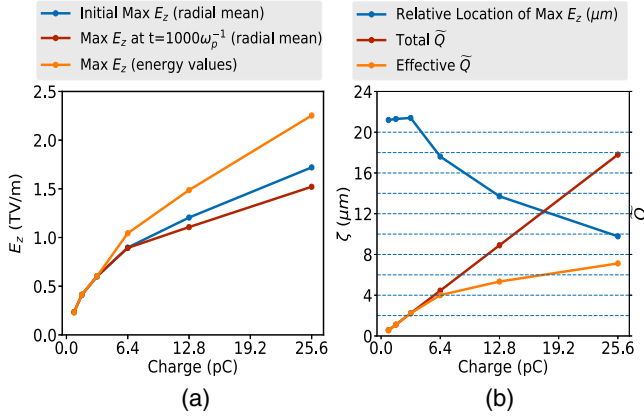


FIG. 4. (a) The variation of initial, final and average maximum axial longitudinal electric fields with charge. The beam is completely bunched and emittance is scaled linearly with charge (3.2 pC \rightarrow 50 nm rad). (b) The location of the peak longitudinal electric field, total and effective normalized charge density \tilde{Q} are also shown. The dashed lines correspond to the position of the bunches.

resonance response is achieved at an earlier point within the microbunch train. This reduces the charge that may be considered to be involved in resonant excitation, and the normalized charge up to this point can be termed as the effective \tilde{Q} . There is a slightly weaker than linear correlation between the effective \tilde{Q} and the maximum longitudinal field in the wake. The fields from higher charge beams are also relatively diminished due to their higher assumed emittances. It can be observed that the use of lower charge beams permits more microbunches to be involved in resonantly driving the wakefields.

For a ten-bunch train, the QNL resonance is found to be sustained for \tilde{Q} values as high as 2.23. Since nonlinear effects grow along the length of the train, however, shorter bunch trains will maintain the resonant condition for even higher values of \tilde{Q} . Furthermore, since the introduction of nonlinearities depends on the charge density, increasing the transverse spot size, σ_x , also increases the maximum \tilde{Q} for which resonance is maintained. With these considerations in mind, it is shown that even for \tilde{Q} values considerably above unity, it is possible for the frequency response to remain approximately linear, enabling resonant QNL excitation.

B. Variation with emittance

To isolate its effects, the beam emittance in the simulations was varied while keeping the total beam charge constant at 12.8 pC. The transverse beam spot size was matched with the plasma for each case. The simulation window is $(5 \mu\text{m})^2$ wide and 26 μm long, divided into $1024^2 \times 2048$ cells, respectively. The variation of maximum longitudinal fields and maximum energy gradients with emittance are plotted in Fig. 5. The average field

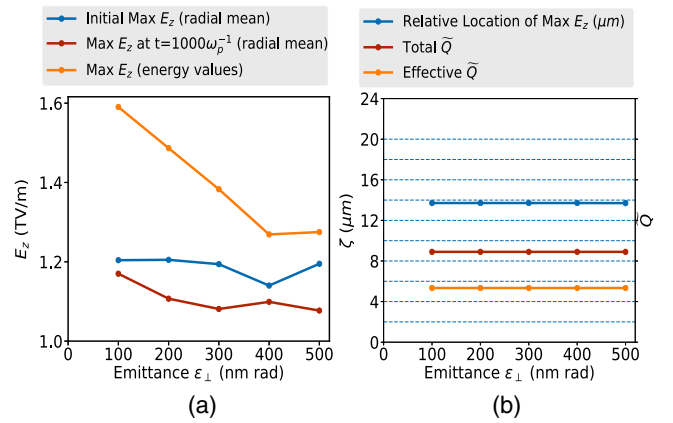


FIG. 5. (a) The variation of initial, final and average maximum axial longitudinal electric fields with emittance. The beam is completely bunched and beam charge is kept constant at 12.8 pC. (b) The location of the peak longitudinal electric field, total and effective normalized charge density \tilde{Q} are plotted. The dashed lines correspond to the position of the bunches.

gradient tends to decrease with increasing emittance, as expected. This is mainly due to the increase in spot size, which decreases the peak beam density, resulting in a weaker plasma wake.

IV. PARTIALLY BUNCHED SYSTEMS

The density modulation given by simple application of IFEL microbunching is only approximately as described above. Indeed, without use of more elaborate approaches [27], the microbunching achieved will be partial, with non-negligible current forming a pedestal between microbunches, which are approximated here as a series of Gaussian pulses. Thus, practical considerations drive the need to understand the complications and possible advantages introduced in the resonant plasma wakefield system by imperfect, or partial, bunching.

The partially bunched system described in Table II was simulated for a time equal to $\frac{5000}{\omega_p}$, i.e., a distance of about 1.59 mm, with results shown in Fig. 6. The resonant PWFA interaction remains stable for this duration. The beam bunch train is initially uniformly bunched and focused, but assumes a density structure as it propagates that ramps upward with distance from the head of the train. This ramping is due to stronger focusing of the trailing bunches induced, as seen before, by the higher on-axis ion density after the onset of ion motion. The maximum energy change was observed to be 905 MeV corresponding to an average accelerating gradient of 0.57 TeV/m. The tail of the beam, i.e., a part of the unbunched beam component, was employed as the witness beam to enable this calculation of energy change.

A. Variation with bunching factor

The systematic relationship between the beam and plasma responses and the degree of microbunching is important to understand, due to both the practical difficulty of approaching full bunching, as well as possible

TABLE II. Table of parameters for the simulation shown in Fig. 6.

Parameter	Value
Total beam charge, Q_b	4.21 pC
Beam energy, E_b	10 GeV
Number of bunches, m	10
Charge distribution	See Fig. 6(a) ($B = 0.71$)
Beam spot size, σ_x	14.6 nm
Normalized transverse emittance, γe_\perp	66 nm rad
Plasma ion species	H ⁺
Plasma density, n_0	$2.79 \times 10^{20} \text{ cm}^{-3}$
Plasma particles per cell	4
Simulation window	$(2.4 \mu\text{m})^2 \times 26 \mu\text{m}$
Resolution	$(2.34 \text{ nm})^2 \times 12.7 \text{ nm}$

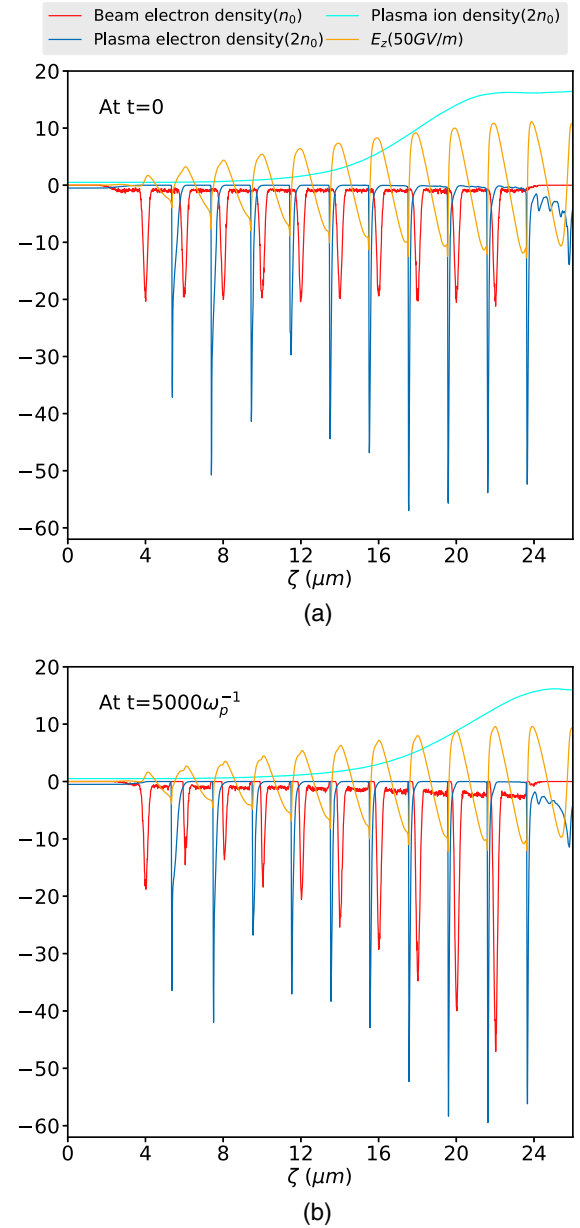


FIG. 6. Beam charge density, plasma density, and longitudinal electric field of a partially bunched system (ratio between peak and flat region ≈ 20) initially (a) and after $t = \frac{5000}{\omega_p}$ (b).

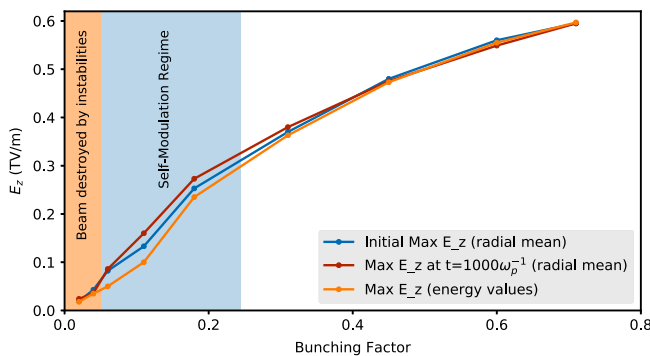
advantages due to incomplete bunching. A common figure of merit for microbunching is the *bunching factor*, defined as $B = \sum e^{i\theta_n} / N_b$, where θ_n are the particle longitudinal phases at a selected wave number [28]. This quantity is equal to zero in the case of a uniformly distributed beam and tends to unity in the limit of a beam ideally microbunched at the bunching wavelength. The variation of the longitudinal electric fields with bunching factor is shown in Fig. 7 along with different regimes of operation detailed below. Generally, the transverse and longitudinal fields are larger at higher bunching factors due to the enhancement of the perturbing beam density and the strengthening of

TABLE III. Table of parameters for the simulation shown in Fig. 8.

Parameter	Value
Total beam charge, Q_b	4.21 pC
Beam energy, E_b	10 GeV
Number of bunches, m	10
Charge distribution	See Fig. 8(a) ($B = 0.11$)
Beam spot size, σ_x	14.6 nm
Normalized transverse emittance, γe_{\perp}	66 nm rad
Plasma ion species	H ⁺
Plasma density, n_0	$2.79 \times 10^{20} \text{ cm}^{-3}$
Plasma particles per cell	4
Simulation window	$(2.4 \mu\text{m})^2 \times 26 \mu\text{m}$
Resolution	$(2.34 \text{ nm})^2 \times 12.7 \text{ nm}$

frequency content of the microbunch train at the resonant frequency. Additionally, with stronger bunching the phase slippage observed in the wake wave (discussed in greater detail below) is reduced, preserving the stable interaction over greater distances.

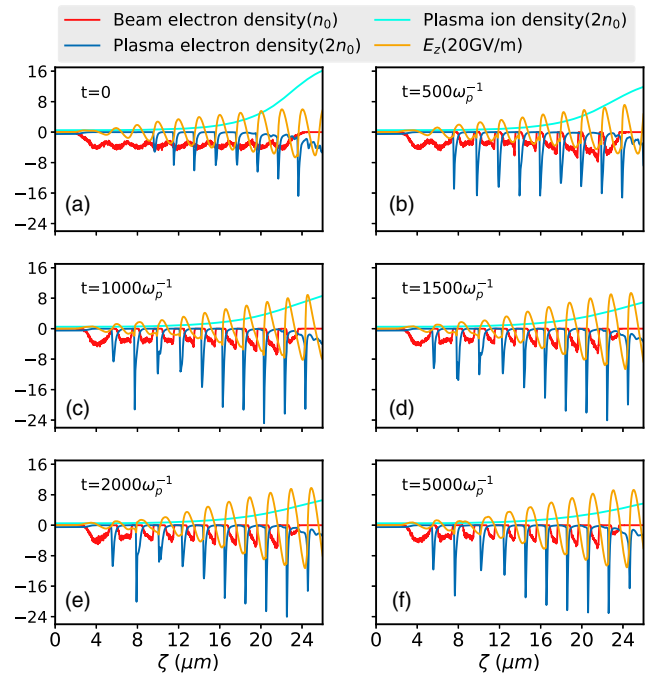
Partial microbunching may also be viewed as similar to seeded self-modulation [29] as it allows one unstable mode to be preferentially excited in the beam-plasma system. If the bunching factor is sufficiently high ($B \gtrsim 0.05$), a self-modulating mode grows, continuing to modulate the beam profile and increasing the bunching factor further. Specifically, this process initiates early in the beam-plasma interaction, with the plasma electrons being completely ejected near the head of the beam [see Fig. 8(a)], leaving an electron-rarefied column several λ_p in length. As the interaction proceeds, however, plasma electrons are attracted back into the region near the axis by the ion column's radial field. This in turn causes defocusing of beam electrons located far from the nominal bunching phase. This in turn increases the beam's bunching factor by ejecting beam electrons radially outward into a halo distribution. In the process, this serves to reduce the on-axis ion density. The feedback loop just described, termed


 FIG. 7. The variation of initial, final and average maximum axial longitudinal electric field with bunching factor, B .

the self-modulation instability (SMI), is convective and is therefore stronger with further distance from the head of the beam [30]. Simulations were performed to examine the growth of this instability using parameters described in Table III and it is illustrated in Fig. 8; SMI-induced effects ultimately approach a quasisteady state where the beam and plasma profile evolution slows down over the duration of the simulation, $5000/\omega_p$.

It should also be noted, however, that at lower initial bunching factors, other instabilities may destroy the beam before SMI can grow to produce such a stable beam profile [30]. For beams with bunching factors slightly below what is determined to be the stable SMI threshold ($0.03 \lesssim B \lesssim 0.05$), the preferred SMI modulation mode does not dominate, and other modes can develop. The effects of these other modes have been previously explored [31]; one such effect is that defocusing regions slip backwards along the beam, ultimately ejecting all beam electrons not contained within the leading bunch. A snapshot of this process is shown in Fig. 9(a) for a beam with $B = 0.04$.

At very low bunching factors ($B \lesssim 0.03$) the beam is effectively a long, nearly uniform beam. Since the growth rates of SMI and the *hosing instability* are comparable [32], with only weak seeding of SMI, the hosing instability may


 FIG. 8. Self-modulation regime ($B = 0.11$); the axial longitudinal electric fields (yellow), beam densities (red), and plasma densities (blue) are shown at times (a) 0, (b) $500/\omega_p$, (c) $1000/\omega_p$, (d) $1500/\omega_p$, (e) $2000/\omega_p$, and (f) $5000/\omega_p$. Initially, plasma electrons are unable to form voids in the beam (a). As the beam propagates, the self-modulation instability forms these voids (e) and resonance is maintained for a long duration (f). Notice, the amplification of the electric fields and the backward shift of the plasma wake with time.

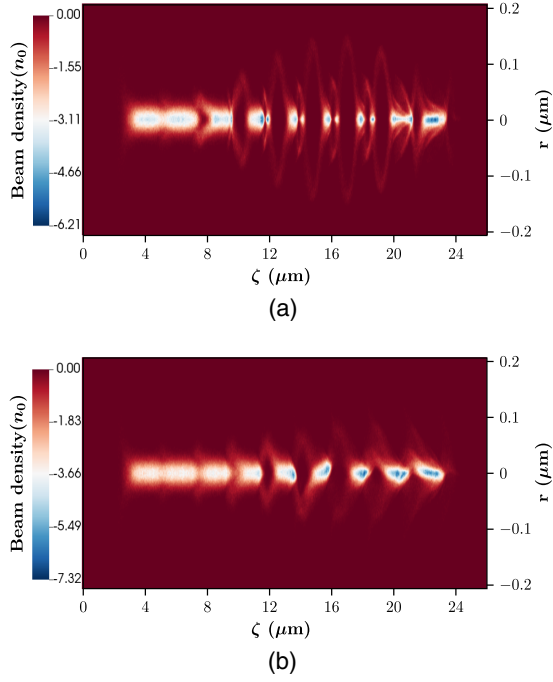


FIG. 9. Observed beam destruction due to phase shifting of the plasma wake at $B = 0.04$ (a) and hosing instability at $B = 0.02$ (b).

also manifest itself and contribute to the prompt destruction of the beam. Both SMI and the hosing instability are evident in Fig. 9(b) for a beam having initial bunching factor $B = 0.02$. Hosing can also manifest more slowly in cases where bunch formation by SMI initially dominates (e.g., $0.05 \lesssim B \lesssim 0.11$); stronger bunching factors can delay the onset of the effect.

B. Variation with charge, partially bunched case

Here we examine the dependence of the longitudinal fields on beam charge in the context of a partially bunched beam. The bunching factor was held constant at $B = 0.71$, keeping the ratio between the peak and flat region densities constant at about 20. As before, the beam emittance was scaled linearly with charge. The simulation window width was changed to 1.2, 1.8, 4, 4, 5 and 5 μm for the beams with charges of 1.03, 2.06, 8.62, 12.8, 17.38, and 25.57 pC, respectively. The variations of the fields are shown in Fig. 10. The effects of higher charge on the fields are similar to the fully bunched case (Fig. 4), but the slope of the final field with respect to charge is shallower due to the effects of the flat-current pedestal. The voids formed in the beam due to the plasma electrons' return to the axis are less pronounced at higher charges due to the steeper longitudinal dependence of the plasma wake. The values of effective \bar{Q} increase with larger charge microbunches and, as before, the resonance eventually saturates. However, this saturation occurs at lower \bar{Q} than in the completely bunched case. This illustrates that, while the accelerating

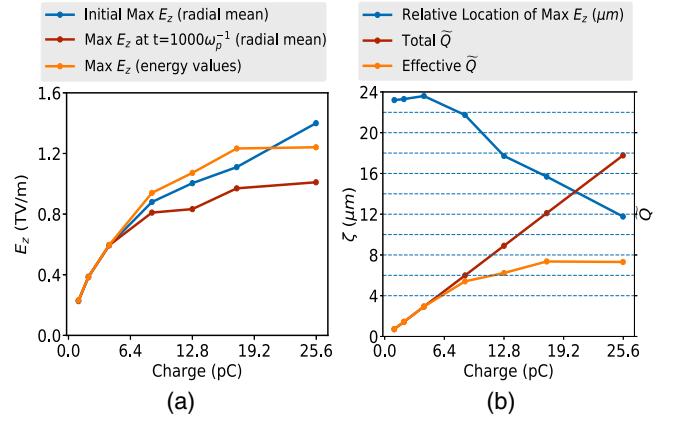


FIG. 10. The variations of initial, final and average maximum axial longitudinal electric fields with charge are plotted in (a). Beam is partially bunched ($B = 0.71$) and the current ratio between the peak and flat region ≈ 20 . Emittance is scaled linearly with charge (3.2 pC \rightarrow 50 nm rad). The location of the peak longitudinal electric field, total and effective normalized charge density \bar{Q} are plotted in part (b). The dashed lines correspond to the positions of the bunches.

field achieved by a realistic, partially bunched beam is substantially similar to the idealized, fully bunched case, there is a reduced incentive to pursue higher charge microbunch operation due to the diminishing returns arising from quicker saturation.

V. OTHER INSTABILITIES IN RESONANT EXCITATION

As we have seen, the resonant beam-plasma system has interdependencies between the electron microbunches and the plasma response, leading to both stable interactions as well as unstable scenarios. Several dominant instabilities arise from the loss of charge in the microbunches and the phase shifting of the plasma wake, both of which can manifest in high B cases. To illustrate these issues, we show in Fig. 1 the additive increase in the plasma bubble dimensions and plasma electron density after each bunch. The first instability, namely defocusing-driven charge loss, results from the ejection of parts of the drive bunches that are near the regions of high plasma electron density, reducing both the beam charge and the strength of E_z . The second, related, instability is phase shifting, which originally initiates due to head erosion of the leading microbunch. As this microbunch loses effective charge, there is a decrease in the plasma electron perturbation causing a backwards shift of the wake (negative ζ). The second microbunch begins to experience a defocusing force, reducing its charge and propagating the instability back along the rest of the bunch train. This same effect also manifests if the plasma wavelength is not well matched with the bunch spacing (due, e.g., to plasma density longitudinal variations). For a well-matched microbunch

train, this instability can be mitigated by the use of lower emittances, and by employing a “pilot” focusing mechanism for the first bunch to mitigate the initiation of head erosion. This pilot may be formed by a preceding intense laser pulse or a leading, tailored component of the electron beam.

Incomplete bunching can also be used to produce a nearly flat region of pedestal current at the front of the bunch train to serve as the pilot beam. This section of the beam produces ion channel focusing fields which help slow the erosion of the more sensitive, leading microbunch, helping to diminish the growth rate of the phase shifting instability. This scenario has been studied through simulations, with an example shown in Figs. 6(a) and 6(b) which includes the onset of head erosion effects. The resonant PWFA system here was also simulated without the pilot component. Although the initial fields were higher in the large- B case, they decreased much more quickly due to head erosion. For comparison, the case without the pilot was simulated for the same, short propagation distance (1.59 mm) and exhibited a maximum energy gain of 895 MeV, corresponding to an average gradient of 563 GeV/m, marginally lower than the pilot-free case. The noted possible improvements obtained from the pilot section must be weighed against the instabilities potentially present in partially bunched systems. Additionally, if the plasma is to be formed by beam-based ionization, the pilot may not be sufficient to completely ionize the plasma. Although a partially ionized plasma will still exert beneficial focusing on the leading microbunch, it is not as effective, and supplementation with another ionization method, such as a leading laser pulse, may be desirable.

VI. WITNESS BEAM INJECTION

The dimensions of the plasma bubble created by optically microbunched beams are notably smaller than the accelerating region currently found in PWFA experiments. If the beam is perfectly microbunched by the IFEL process, the rearmost drive beam bunch could be used as a witness, provided that the plasma blowout is sufficiently elongated to encompass a major portion of the bunch in the accelerating phase. This has been observed in the case of higher charge bunches where the saturation of the resonance response is achieved at an earlier position. If the beam is not fully microbunched, the electrons in the flat pedestal of the current profile may be trapped by the large accelerating wakefields, forming a self-injected witness train. A smaller bunching factor obviously leaves a larger number beam electrons available for injection, but a relatively small fraction would be trapped at accelerating phases. Additionally, since electrons in the pedestal are by definition diffuse in phase, the longitudinal phase space area spread of a self-injected witness would be relatively large. The injection process in the specific case from Fig. 6 is shown in detail in Fig. 11, illustrating the acceleration of

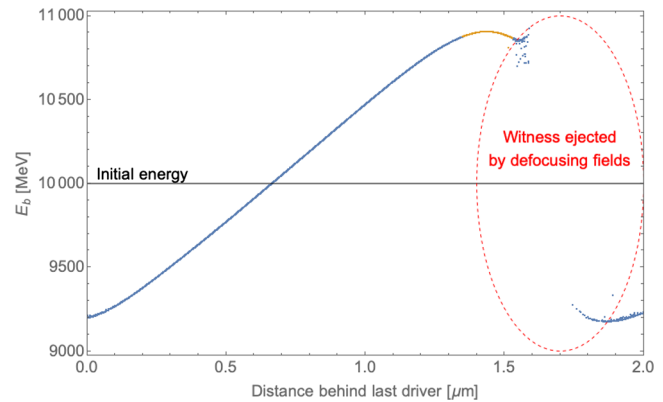


FIG. 11. Final longitudinal phase space of the current pedestal trailing the last driver bunch. The accelerated beam has a core region, shown in orange, with the following parameters: 0.1% rms energy spread, 10.2 fC charge, 178 nm total length, 127 nm rad normalized emittance.

the current pedestal in the region trailing the last driver bunch. A 0.1% rms energy spread beam core (in orange) containing 10.2 fC of charge over 178 nm length is accelerated to a mean energy of 10.9 GeV, with a normalized emittance of 127 nm rad. Despite the crudeness of this injection method, this beam has a 6D brightness competitive with that of current frontier FEL injectors [11].

While this is a promising performance, as a future refinement, laser induced ionization injection, such as the Trojan Horse, or plasma photocathode, technique [33,34], may be used to produce a brighter witness beam. The plasma photocathode method is challenging in a number of ways. First, the ionized region is not small compared to the bubble. Further, in the QNL regime, the wakefield amplitude may be somewhat below wave breaking (here we observe in simulations that it is $<0.4 \times E_{WB}$), which implies that while trapping can occur, it is permitted over a restricted range of wave phases.

VII. BEAM-INDUCED FIELD IONIZATION

Beam-based ionization is a critical topic for a very high field scenario of resonant PWFA excitation using optically microbunched beams. This is owed to the fact that space-charge fields near these extremely strongly focused, very high brightness electron microbunches are near the TV/m level. This field is large enough to ionize the plasma in a few femtoseconds [35]. Such fast ionization has been confirmed in simulations using FBPIC (a spectral, quasi-3D PIC code) [36], where the plasma is indeed formed within a few femtoseconds of beam passage. The plasma wake formed in this case is shown in Fig. 12. The rate of ionization probability [37] implemented in FBPIC follows the Ammosov-Delone-Krainov (ADK) tunneling ionization model [38]. The gas used in these simulations was hydrogen, in order to avoid multiple ionization. The first microbunch of the partially bunched beam was used in this

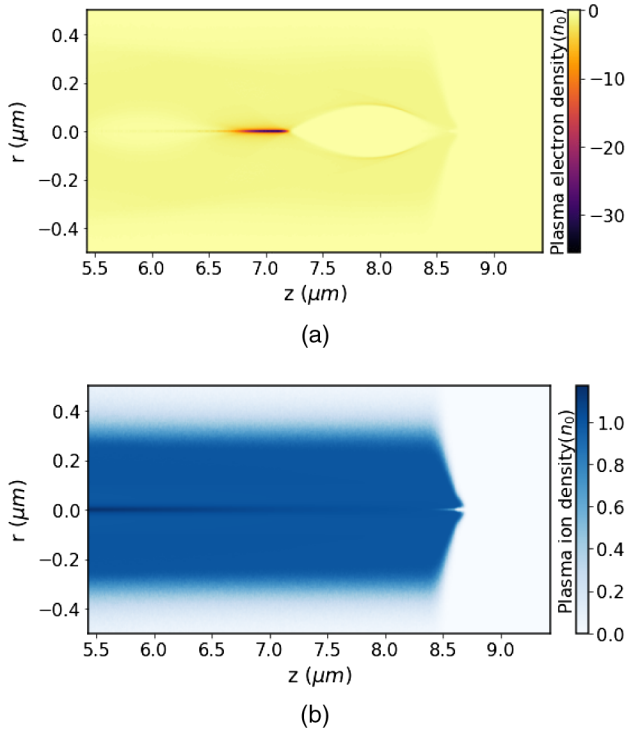


FIG. 12. The plasma electrons (a) and protons (b) created by the field ionization of hydrogen gas by a single electron bunch positioned at $z = 8.44 \mu\text{m}$ (charge per bunch = 0.32 pC , $\sigma_x = 13 \text{ nm}$, $\sigma_z = 110 \text{ nm}$).

simulation to demonstrate the efficacy of the ionization process. The radial size of the simulation box is $1 \mu\text{m}$ and the longitudinal size is $4 \mu\text{m}$, divided into 383×1532 cells respectively, with 64 particles per cell distributed as $4 \times 4 \times 4$ in the longitudinal, radial and azimuthal directions, respectively. The simulations were performed with a single azimuthal mode ($m = 0$) and the time step for the simulations is $0.011/\omega_p$.

It should be noted that for our experimental parameters, the beam fields may cause ionization of atomic species in the barrier suppression ionization (BSI) regime [39] wherein electrons are classically permitted to escape from the nuclear potential, and tunneling is no longer a relevant concept. This effect allows the plasma wake to be formed even more quickly than indicated by tunneling models, further reducing head erosion in the case that the gas is not preionized. This fast ionization process may obviate the need to preionize the gas. However, there are two major obstacles to reliance on BSI to speed up the foreseen ionization rate over that obtained from ADK predictions. The first is conceptual: the BSI regime is still not theoretically well understood, since it requires a nonperturbative approach. Likewise, BSI in unipolar cases (particle beamlike) has not been experimentally benchmarked. In the second consideration, for the leading edge of the beam, the threshold for full ionization via BSI may not be reached after the onset of head erosion. In this case the faster process of BSI gives way to tunneling

in self-ionized scenarios [40]. To avoid this effect, preionization may still be desirable.

VIII. DISCUSSION AND OUTLOOK FOR FACET-II EXPERIMENTS

The experimental realization of TV/m plasma wakefields through *single bunch*, low emittance beam excitation has been discussed in some detail in Ref. [35]. Here we have presented and discussed in some detail an alternative path to achieving TV/m wakes, through a quasinonlinear resonant excitation mechanism. A key advantage here is shared with the application of very low emittance beams to driving an x-ray FEL—the final compression of the beam (which yields resonance in a very high density plasma in the QNL regime) is performed via the IFEL process. This permits obtaining of very high peak current while avoiding many of the deleterious effects of conventional compression, such as induced emittance growth and energy spread. Emittance growth is particularly damaging, as it limits the peak beam density attainable to drive plasma wakefields in the QNL regime, and exacerbates issues such as head erosion. Experimental preparation in both QNL PWFA and x-ray FEL cases begins with the creation of the beam, and in this regard it is noted that since the time of the experiments reported in Ref. [41], and the initial analysis of [35], that significant improvements in the approach to obtaining higher brightness electron beams have been introduced, e.g., Ref. [11]. Indeed, in [11], an analysis of IFEL-induced microbunching for ultrahigh brightness, 10 GeV-class beams (as would be employed for FACET-II experiments [42]) has already been performed. The efficacy of IFEL microbunching has further been validated by the successful results of the XLEAP experiment at SLAC [2], with the achievement of high brightness microbunches verified through the generation of attosecond x-ray FEL pulses. To enable the experimental cases analyzed here, one must introduce, in addition to a high brightness electron source, a laser modulation and bunching system as employed in XLEAP.

After creation, acceleration, compression and microbunching of the electron beam at FACET-II, the beam must be focused to very small spot sizes, sub-mm at these high plasma densities [35]. This can be accomplished using very high gradient (700 T/m, or higher) permanent magnet quadrupoles that are tens of cm in length, and tuned via changing their relative longitudinal positions [9]. Such a focusing system will also be needed for the FACET-II experiment E-314 on ion motion, with its attendant search for formation of a mutually focused ion and beam electron equilibrium profile [43]. Alternatively, one may use an underdense plasma lens for the final focusing element, as already proposed for FACET-II [44], with implementation now being initiated.

The beam size at final focus may be deduced from appearance intensity [35], and ionization yield in the gas,

which is to be supplied in FACET-II experiments by nozzle jets to achieve several mm of multiatmosphere pressure hydrogen. Alternatively, with an optically microbunched beam, one may employ coherent diffraction imaging (CDI) based methods to reconstruct the suboptical beam profiles. This is due to the tight bunching employed, which can give high harmonics of the bunching period in coherent emission processes (e.g., edge radiation, plasma-based transition radiation). This short wavelength light can permit coherent imaging reconstruction, thus extending the IFEL-based CDI beam profile measurements reported in Ref. [45] to smaller spot sizes. Once established, the beam-plasma interaction can be interrogated by the measurement of the betatron radiation spectrum. An example of such a spectrum, for a case without hosing or ion collapse, is shown in Fig. 13. The radiation spectrum in this preliminary analysis is quite hard, extending to beyond 100 MeV, due to the very high plasma density and concomitant focusing strength. Studies of the changes to this spectrum due to instabilities and attendant larger amplitude betatron motion are now under way.

Many diagnostic systems needed for characterizing the beam will be available at FACET-II [8,44]. These include: the betatron radiation spectrum via a Compton/pair spectrometer, as described in Ref. [46]; the downstream beam imaging systems to determine phase space dilution of accelerated beams in this case [47]; and momentum-resolving spectrometers. It should be noted that this experiment, along with that aimed at demonstrating the development of ion-electron beam Bennett equilibria, should be the first investigations to unequivocally access a regime of nontrivial ion motion, a critically important effect in linear collider applications of PWFA [48,49]. In addition to observable focal effects on the beam, and related betatron radiation signatures, it is proposed to instrument the interaction region with a keV-range ion retarding energy analyzer.

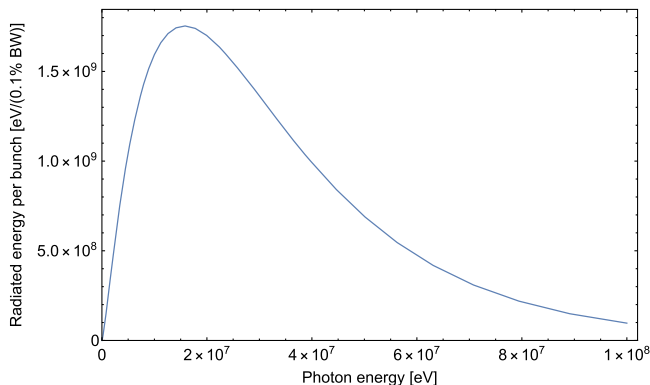


FIG. 13. Betatron radiation emitted by a single electron bunch (charge = 0.32 pC, $\sigma_x = 13$ nm, $\sigma_z = 110$ nm) as it propagates a distance of 1.6 mm with $n_i = n_0$; ion collapse effects are not included.

The existence of independent witness beams at FACET-II are a key feature of the new facility, which should be exploited for injection studies in this system. Injection may also be accomplished by detuning the energy of the beam tail to prevent effective microbunching in this region. This would permit the loading of electrons at a full range of initial phases, leading to a large fraction of witness beam electrons being captured and accelerated.

The issues to be explored in this proposed FACET-II experimental program are myriad. The effects of the bunching factor are of particular interest, as they may influence beam stability, head erosion dynamics, and wakefield excitation efficiency. The evolution of partially bunched systems through the various mechanisms discussed here provide an ideal platform for investigating beam seeded self-modulation in plasmas. It also provides a sensitive system to investigate head erosion and methods for its mitigation, including an experimental comparison between self-ionized and laser-ionized performance [50]. We note that the FACET-II tests permit an experimental investigation of limits on total acceleration. For the first experiments, we intend to limit the beam propagation length in plasma to the few mm range, implying 1 GeV maximum energy shift. Expanding this interaction length towards the cm level permits exploration of the maximum acceleration derived from possible beam instabilities—as discussed above—as well as pump depletion.

Beyond quasinonlinear resonance occurring when the beam is microbunched at a spacing of λ_p , more sophisticated schemes may also be tested. One such variation utilizes a linearly ramped beam current that is microbunched at spacing of $1.5\lambda_p$. This scheme may permit a large transformer ratio to be reached [51]. It would, however, enhance ion collapse and could lead to instabilities due to self-modulation of the beam structure at λ_p . Such experimental possibilities will be investigated theoretically to evaluate the feasibility of their implementation.

The studies presented here have assumed bunching with a near-IR ($2 \mu\text{m}$ wavelength) laser. This choice was motivated by the desire to access TV/m-class fields using a resonantly excited PWFA system. This choice in turn places stringent demands on beam quality, and scales all parameters involved in the experiment downward in size—notably the transverse emittance and beam sizes. Further, operation with gas and attendant plasma densities close to cutoff for ionizing lasers would introduce challenging focal and propagation effects should a laser be used in the experiment. To mitigate experimental challenges introduced by this scaling, one may use a longer wavelength laser, e.g., $10 \mu\text{m}$, permitting higher emittance, higher charge beams to be used, while employing notably lower plasma density. This choice would lower the field expected to the few 100 GV/m range, which are still of notably high interest.

In conclusion, the resonant excitation of PWFA with an optical-IR period microbunch train promises to be a robust alternative for accessing TV/m-class plasma wakefields. This initiative takes advantage of recent experimental progress in microbunch creation in high brightness electron beams at multi-GeV energy. Further, with small modifications to existing infrastructure at FACET-II, experimental parameters relevant to E-317 described here will be enabled. In this regard, we note that the use of microbunched beams with attosecond structure are also needed for E-318, an ultrafast atomic physics experiment planned for FACET-II. This experiment, which can uniquely explore atomic electron dynamics under the influence of TV/m unipolar electric fields, is highly synergistic with the PWFA experiments described above, exploring effects which may be exploited as diagnostics in E-317.

ACKNOWLEDGMENTS

This work was performed with support of the U.S. Department of Energy, Division of High Energy Physics, under Contract No. DE-SC0009914 and National Science Foundation under Grant No. PHY-1549132. This work used computational and storage services associated with the Hoffman2 Shared Cluster provided by UCLA Institute for Digital Research and Educations Research Technology Group and the SCARF cluster provided by the STFC Scientific Computing Department.

-
- [1] J. B. Rosenzweig, B. Breizman, T. Katsouleas, and J. J. Su, Acceleration and focusing of electrons in two-dimensional nonlinear plasma wakefields, *Phys. Rev. A* **44**, R6189 (1991).
- [2] J. Duris, S. Li, T. Driver, E. G. Champenois, J. P. MacArthur, A. A. Lutman, Z. Zhang, P. Rosenberger, J. W. Aldrich, R. Coffee *et al.*, Tunable isolated attosecond x-ray pulses with gigawatt peak power from a free-electron laser, *Nat. Photonics* **14**, 30 (2020).
- [3] J. Rosenzweig, G. Andonian, M. Ferrario, P. Muggli, O. Williams, V. Yakimenko, and K. Xuan, Plasma wakefields in the quasinonlinear regime, *AIP Conf. Proc.* **1299**, 500 (2010).
- [4] S. Barber, Plasma Wakefield Experiments in the Quasi Nonlinear Regime, Ph.D. thesis, University of California, Los Angeles, 2014.
- [5] J. Rosenzweig, G. Andonian, S. Barber, M. Ferrario, P. Muggli, B. O'Shea, Y. Sakai, A. Valloni, O. Williams, Y. Xi, and V. Yakimenko, Plasma wakefields in the quasinonlinear regime: Experiments at ATF, *AIP Conf. Proc.* **1507**, 612 (2012).
- [6] E. Parra, S. J. McNaught, and H. M. Milchberg, Characterization of a cryogenic, high-pressure gas jet operated in the droplet regime, *Rev. Sci. Instrum.* **73**, 468 (2002).
- [7] N. Barov and J. B. Rosenzweig, Propagation of short electron pulses in underdense plasmas, *Phys. Rev. E* **49**, 4407 (1994).
- [8] V. Yakimenko, L. Alsberg, E. Bong, G. Bouchard, C. Clarke, C. Emma, S. Green, C. Hast, M. J. Hogan, J. Seabury *et al.*, FACET-II facility for advanced accelerator experimental tests, *Phys. Rev. Accel. Beams* **22**, 101301 (2019).
- [9] J. K. Lim, P. Frigola, G. Travish, J. B. Rosenzweig, S. G. Anderson, W. J. Brown, J. S. Jacob, C. L. Robbins, and A. M. Tremaine, Adjustable, short focal length permanent-magnet quadrupole based electron beam final focus system, *Phys. Rev. ST Accel. Beams* **8**, 072401 (2005).
- [10] P. Chen, K. Oide, A. M. Sessler, and S. S. Yu, Plasma-Based Adiabatic Focuser, *Phys. Rev. Lett.* **64**, 1231 (1990).
- [11] J. B. Rosenzweig, A. Cahill, V. Dolgashev, C. Emma, A. Fukasawa, R. Li, C. Limborg, J. Maxson, P. Musumeci, A. Nause *et al.*, Next generation high brightness electron beams from ultrahigh field cryogenic rf photocathode sources, *Phys. Rev. Accel. Beams* **22**, 023403 (2019).
- [12] E. Marin, A. Latina, R. Tomás, and D. Schulte, Final focus system tuning studies towards compact linear collider feasibility, *Phys. Rev. Accel. Beams* **21**, 011003 (2018).
- [13] S. Augst, D. D. Meyerhofer, D. Strickland, and S. L. Chin, Laser ionization of noble gases by Coulomb-barrier suppression, *J. Opt. Soc. Am. B* **8**, 858 (1991).
- [14] A. Cahill, A. Fukasawa, R. Pakter, J. Rosenzweig, V. Dolgashev, C. Limborg, S. Tantawi, S. Bruno, and G. Castorina, Rf design for the topgun photogun: A cryogenic normal conducting copper electron gun, *Nucl. Instrum. Methods Phys. Res., Sect. A* **865**, 105 (2016).
- [15] J. MacArthur, J. Duris, Z. Huang, and A. Marinelli, High power subfemtosecond x-ray pulse study for the LCLS, in *Proceedings of the 8th International Particle Accelerator Conference (IPAC 2017), Copenhagen, Denmark, 2017* (JACoW Publishing, Geneva, Switzerland, 2017), WE-PAB118.
- [16] C. Huang, V. Decyk, C. Ren, M. Zhou, W. Lu, W. Mori, J. Cooley, T. Antonsen, and T. Katsouleas, QUICKPIC: A highly efficient particle-in-cell code for modeling wakefield acceleration in plasmas, *J. Comput. Phys.* **217**, 658 (2006).
- [17] E. Hemsing, G. Stupakov, D. Xiang, and A. Zholents, Beam by design: Laser manipulation of electrons in modern accelerators, *Rev. Mod. Phys.* **86**, 897 (2014).
- [18] J. Duris, M. Babzien, M. Fedurin, K. Kusche, R. K. Li, J. Moody, I. Pogorelsky, M. Polyanskiy, J. B. Rosenzweig, Y. Sakai *et al.*, High-quality electron beams from a helical inverse free-electron laser accelerator, *Nat. Commun.* **5**, 4928 (2014).
- [19] Y. Liu, X. J. Wang, D. B. Cline, M. Babzien, J. M. Fang, J. Gallardo, K. Kusche, I. Pogorelsky, J. Skaritka, and A. van Steenberg, Experimental Observation of Femtosecond Electron Beam Microbunching by Inverse Free-Electron-Laser Acceleration, *Phys. Rev. Lett.* **80**, 4418 (1998).
- [20] W. Lu, C. Huang, M. Zhou, W. B. Mori, and T. Katsouleas, Nonlinear Theory for Relativistic Plasma Wakefields in the Blowout Regime, *Phys. Rev. Lett.* **96**, 165002 (2006).
- [21] E. Kallos, P. Muggli, T. Katsouleas, V. Yakimenko, D. Stolyarov, I. Pogorelsky, I. Pavlishin, K. Kusche, M. Babzien, I. BenZvi *et al.*, Resonant plasma wakefield experiment: Plasma simulations and multibunched electron beam diagnostics, *AIP Conf. Proc.* **877**, 520 (2006).

- [22] K. V. Lotov, Excitation of two-dimensional plasma wakefields by trains of equidistant particle bunches, *Phys. Plasmas* **20**, 083119 (2013).
- [23] S. Barber, G. Andonian, B. O'Shea, J. Rosenzweig, Y. Sakai, O. Williams, M. Ferrario, and P. Muggli, Quasilinear plasma wakefield acceleration experiments, in *Proceedings of the 27th Linear Accelerator Conference, LINAC2014, Geneva, Switzerland, 2014* (JACoW Publishing, Geneva, Switzerland, 2014), TUPP110.
- [24] N. Barov, J. B. Rosenzweig, M. C. Thompson, and R. B. Yoder, Energy loss of a high-charge bunched electron beam in plasma: Analysis, *Phys. Rev. ST Accel. Beams* **7**, 061301 (2004).
- [25] R. Robles and J. Rosenzweig, Compression of ultrahigh brightness beams for a compact x-ray free-electron laser, *Instruments* **3**, 53 (2019).
- [26] K.-J. Kim, Rf and space-charge effects in laser-driven rf electron guns, *Nucl. Instrum. Methods Phys. Res., Sect. A* **275**, 201 (1989).
- [27] N. Sudar, P. Musumeci, I. Gadjev, Y. Sakai, S. Fabbri, M. Polyanskiy, I. Pogorelsky, M. Fedurin, C. Swinson, K. Kusche, M. Babzien, and M. Palmer, Demonstration of Cascaded Modulator-Chicane Microbunching of a Relativistic Electron Beam, *Phys. Rev. Lett.* **120**, 114802 (2018).
- [28] P. Musumeci, C. Pellegrini, and J. B. Rosenzweig, Higher harmonic inverse free-electron laser interaction, *Phys. Rev. E* **72**, 016501 (2005).
- [29] Y. Fang, V. Yakimenko, M. Babzien, M. Fedurin, K. Kusche, R. Malone, J. Vieira, W. Mori, and P. Muggli, Seeding of Self-Modulation Instability of a Long Electron Bunch in a Plasma, *Phys. Rev. Lett.* **112**, 045001 (2014).
- [30] N. Kumar, A. Pukhov, and K. Lotov, Self-Modulation Instability of a Long Proton Bunch in Plasmas, *Phys. Rev. Lett.* **104**, 255003 (2010).
- [31] K. Lotov, Simulation of ultrarelativistic beam dynamics in the plasma wakefield accelerator, *Nucl. Instrum. Methods Phys. Res., Sect. A* **410**, 461 (1998).
- [32] C. B. Schroeder, C. Benedetti, E. Esarey, F. J. Gruner, and W. P. Leemans, Coupled beam hose and self-modulation instabilities in overdense plasma, *Phys. Rev. E* **86**, 026402 (2012).
- [33] B. Hidding, J. B. Rosenzweig, Y. Xi, B. O'Shea, G. Andonian, D. Schiller, S. Barber, O. Williams, G. Pretzler, T. Knigstein *et al.*, Beyond injection: Trojan horse underdense photocathode plasma wakefield acceleration, *AIP Conf. Proc.* **1507**, 570 (2012).
- [34] A. Deng *et al.*, Generation and acceleration of electron bunches from a plasma photocathode, *Nat. Phys.* **15**, 1156 (2019).
- [35] J. Rosenzweig, G. Andonian, P. Bucksbaum, M. Ferrario, S. Full, A. Fukusawa, E. Hemsing, B. Hidding, M. Hogan, P. Krejcik *et al.*, Teravolt-per-meter beam and plasma fields from low-charge femtosecond electron beams, *Nucl. Instrum. Methods Phys. Res., Sect. A* **653**, 98 (2011).
- [36] R. Lehe, M. Kirchen, I. A. Andriyash, B. B. Godfrey, and J.-L. Vay, A spectral, quasicylindrical and dispersion-free particle-in-cell algorithm, *Comput. Phys. Commun.* **203**, 66 (2016).
- [37] M. Chen, E. Cormier-Michel, C. Geddes, D. Bruhwiler, L. Yu, E. Esarey, C. Schroeder, and W. Leemans, Numerical modeling of laser tunneling ionization in explicit particle-in-cell codes, *J. Comput. Phys.* **236**, 220 (2013).
- [38] V. K. M. V. Ammosov and N. B. Delone, Tunnel ionization of complex atoms and of atomic ions in an alternating electromagnetic field, *J. Exp. Theor. Phys.* **64**, 1191 (1986).
- [39] D. Bauer and P. Mulser, Exact field ionization rates in the barrier-suppression regime from numerical time-dependent Schrödinger-equation calculations, *Phys. Rev. A* **59**, 569 (1999).
- [40] M. Zhou, C. E. Clayton, C. Huang, C. Joshi, W. Lu, K. A. Marsh, W. B. Mori, T. Katsouleas, P. Muggli, E. Oz *et al.*, Beam head erosion in self-ionized plasma wakefield accelerators, in *Proceedings of the 22nd Particle Accelerator Conference, PAC-2007, Albuquerque, NM* (IEEE, New York, 2007), pp. 3064–3066.
- [41] Y. Ding, A. Brachmann, F.-J. Decker, D. Dowell, P. Emma, J. Frisch, S. Gilevich, G. Hays, P. Hering, Z. Huang *et al.*, Measurements and Simulations of Ultralow Emittance and Ultrashort Electron Beams in the Linac Coherent Light Source, *Phys. Rev. Lett.* **102**, 254801 (2009).
- [42] C. Joshi, E. Adli, W. An, C. E. Clayton, S. Corde, S. Gessner, M. J. Hogan, M. Litos, W. Lu, K. A. Marsh, W. B. Mori, N. Vafaei-Najafabadi, B. O'shea, X. Xu, G. White, and V. Yakimenko, Plasma wakefield acceleration experiments at FACET II, *Plasma Phys. Controlled Fusion* **60**, 034001 (2018).
- [43] C. Hansel, M. Yadav, P. Manwani, W. An, W. Mori, and J. B. Rosenzweig, Nonlinear equilibria and emittance growth due to scattering in plasma wakefield accelerators with ion motion, *Phys. Rev. Accel. Beams* (to be published).
- [44] C. E. Doss, E. Adli, R. Ariniello, J. Cary, S. Corde, B. Hidding, M. J. Hogan, K. Hunt-Stone, C. Joshi, K. A. Marsh *et al.*, Laser-ionized, beam-driven, underdense, passive thin plasma lens, *Phys. Rev. Accel. Beams* **22**, 111001 (2019).
- [45] A. Marinelli, M. Dunning, S. Weathersby, E. Hemsing, D. Xiang, G. Andonian, F. O'Shea, J. Miao, C. Hast, and J. B. Rosenzweig, Single-Shot Coherent Diffraction Imaging of Microbunched Relativistic Electron Beams for Free-Electron Laser Applications, *Phys. Rev. Lett.* **110**, 094802 (2013).
- [46] B. Naranjo, Y. Zhang, G. Lawler, W. Lynn, M. Yadav, and J. B. Rosenzweig, MeV through GeV Gamma Diagnostics for FACET II: Compton-Pair Tracker, *Phys. Rev. Accel. Beams* (to be published).
- [47] R. Ariniello, C. E. Doss, K. Hunt-Stone, J. R. Cary, and M. D. Litos, Transverse beam dynamics in a plasma density ramp, *Phys. Rev. Accel. Beams* **22**, 041304 (2019).
- [48] J. B. Rosenzweig, A. M. Cook, A. Scott, M. C. Thompson, and R. B. Yoder, Effects of Ion Motion in Intense Beam-Driven Plasma Wakefield Accelerators, *Phys. Rev. Lett.* **95**, 195002 (2005).
- [49] W. An, W. Lu, C. Huang, X. Xu, M. J. Hogan, C. Joshi, and W. B. Mori, Ion Motion Induced Emittance Growth of Matched Electron Beams in Plasma Wakefields, *Phys. Rev. Lett.* **118**, 244801 (2017).
- [50] W. An, M. Zhou, N. Vafaei-Najafabadi, K. A. Marsh, C. E. Clayton, C. Joshi, W. B. Mori, W. Lu, E. Adli, S. Corde

et al., Strategies for mitigating the ionization-induced beam head erosion problem in an electron-beam-driven plasma wakefield accelerator, *Phys. Rev. ST Accel. Beams* **16**, 101301 (2013).

[51] E. Kallos, P. Muggli, T. Katsouleas, V. Yakimenko, and J. Park, Simulations of a high transformer ratio plasma wakefield accelerator using multiple electron bunches, *AIP Conf. Proc.* **1086**, 580 (2009).